


# Optimizing Cs<sub>2</sub>TiBr<sub>6</sub>-Based PSCs with Graphene Quantum Dots <sup>†</sup>

Riya Sen <sup>1,2,\*</sup>  and Menka Yadav <sup>1</sup>

<sup>1</sup> Department of Electronics & Communication Engineering, Malaviya National Institute of Technical Studies, Jaipur 302017, India; menka.ece@mnit.ac.in

<sup>2</sup> Department of Electronics and Communications Engineering, Geetanjali Institute of Technical Studies, Udaipur 313022, India

\* Correspondence: 2019rec9508@mnit.ac.in

<sup>†</sup> Presented at the 4th International Electronic Conference on Applied Sciences, 27 October–10 November 2023; Available online: <https://asec2023.sciforum.net/>.

**Abstract:** The overall efficiency and optimization of perovskite solar cells are significantly influenced by the selective layers in the cells. In this study, particular emphasis is placed on a perovskite solar cell architecture in which the charge transport layer has been removed from the structure intentionally. In this paper, the full fabrication procedure is given free from the charge transport layer. To understand the behavior of the perovskite material, XRD analysis and TEM analysis, along with photoluminescence measurements, were conducted. These measurements provided valuable insights into the efficiency of the perovskite material. Additionally, SEM analysis was employed to characterize the surface morphology of the proposed structure. Furthermore, the photovoltaic performance of the proposed solar cell architectures was evaluated. With the addition of graphene quantum dots in the perovskite solar cell's structure, we achieved an impressive 1.02% efficiency. These results show that, with a simple manufacturing procedure, removing the charge transport layer would have the greatest influence on photovoltaic performance. Overall, this research is helpful in understanding how cesium titanium bromide functions as an absorber in perovskite solar cells.

**Keywords:** solar cell; cesium; perovskite; charge transport layer free



**Citation:** Sen, R.; Yadav, M. Optimizing Cs<sub>2</sub>TiBr<sub>6</sub>-Based PSCs with Graphene Quantum Dots. *Eng. Proc.* **2023**, *56*, 180. <https://doi.org/10.3390/ASEC2023-15298>

Academic Editor: Simeone Chianese

Published: 26 October 2023



**Copyright:** © 2023 by the authors. Licensee MDPI, Basel, Switzerland. This article is an open access article distributed under the terms and conditions of the Creative Commons Attribution (CC BY) license (<https://creativecommons.org/licenses/by/4.0/>).

## 1. Introduction

Perovskite solar cells (PSCs) excel in the photovoltaics industries, boasting high power conversion efficiency (PCE) and cost-effective manufacturing. Their impressive PCE competes with that of advanced solar technology, promising greener energy. With low-cost, scalable production, PSCs have redefined solar energy's landscape, driving sustainability and affordability in solar power. This remarkable progress has positioned PSCs as formidable competitors to other exciting solar cell technologies [1–3]. The unique properties of perovskite materials, such as broad absorption, a long diffusion length, and solution processability, make them exceptionally suitable as efficient light harvesters in PSCs [4–6]. PSCs can be categorized into three main architectures: planar, mesoporous, and inverted-structure. An additional potential function of some solar cells is the elimination of the HTL, the ETL, or even both. In such cases, the perovskite layer must perform the dual role of being a light harvester and a hole or electron conductor. The limited exploration of this simplest PSC configuration without ETL or HTL may have stemmed from the complications faced by this device structure, particularly in terms of perovskite film deposition and charge extraction [7]. Addressing these issues, Tang et al. successfully designed the simplest PSC (FTO/CsPbBr<sub>3</sub>/carbon), wherein CsPbBr<sub>3</sub> served as the light-absorbing material. Modifying the FTO/CsPbBr<sub>3</sub> specially with CsPbBr<sub>3</sub> quantum dots and using porous FTO and NiO-incorporated MAPbI<sub>3</sub> in this PSC boosted the PCE to 4.1% [8]. Xiong et al. optimized a basic MAPbI<sub>3</sub>-based PSC by introducing porous FTO and NiO within the perovskite layer [9]. Developing HTL- or ETL-free PSCs presents specific challenges. The

absence of dedicated ETL or HTL leads to a heightened energy level difference between the perovskite layer and the metal contact or FTO glass, potentially causing recombination issues. The inherent electronic properties of materials must be optimized to compensate for the missing layers and ensure efficient charge carrier extraction. Additionally, careful solvent engineering is crucial to preventing solvent-related harm to underlying layers. These considerations are essential for achieving a stable and high-performance ETL- or HTL-free perovskite solar cell.

In this study, we initially introduced and explored an ETL- and HTL-free PSC device structure consisting of FTO/ $\text{Cs}_2\text{TiBr}_6$ /silver, achieving a PCE of 0.89%. Subsequently, by incorporating graphene quantum dots (GQDs) into the FTO/ $\text{Cs}_2\text{TiBr}_6$ /Ag structure, we enhanced the PCE to 1.02% under simulated AM 1.5G solar illumination. Furthermore, we delved into the characteristics of  $\text{Cs}_2\text{TiBr}_6$  (a lead-free perovskite material) and examined its potential as a visible-light absorber for photovoltaic applications. The structure of this paper is as follows: Section 2 comprehensively covers the design and fabrication process of the PSC; Section 3 details the outcomes of our investigation; and lastly, Section 4 provides the concluding remarks.

## 2. Fabrication and Design of Proposed PSC Structure

### 2.1. Synthesis of $\text{Cs}_2\text{TiBr}_6$ and PSC Structure (FTO/ $\text{Cs}_2\text{TiBr}_6$ /Silver)

To synthesize the  $\text{Cs}_2\text{TiBr}_6$ , a solution with di-isopropoxide bis(acetylacetonate) (TDBA; 50  $\mu\text{L}$ , 0.10 mmol),  $\text{Cs}_2\text{CO}_3$  (35 mg, 0.10 mmol), oleylamine (OIAM; 0.60 mL), and oleic acid (OA; 1.0 mL) was mixed. After 2 h of vacuum-assisted reflux in a 25 mL round-bottomed flask for dryness, magnetic stirring at 330 RPM removed impurities, aiding  $\text{Cs}_2\text{TiBr}_6$  nanocrystal synthesis. Following the precursory preparation, quick TMS-Br (0.6 mL) injection at varying temperatures (90, 135, 185, and 245  $^\circ\text{C}$ ) under argon gas darkened the solution. Maintaining the injection temperature for 10 to 12 s controlled the nanocrystal growth. Rapid cooling with an ice-water bath halted this growth, and centrifugation at 5000 rpm for 4 min separated the  $\text{Cs}_2\text{TiBr}_6$  nanocrystals from the precipitate. Dissolving the precipitate in 2 mL of hexane enhanced its stability and solubility. The colloidal solution was stored in a glovebox to prevent unintended reactions or contamination until later use in experiments or applications [10].

The complete PSC was fabricated using a straightforward spin-coating technique, as shown in Figure 1. Perovskite material was spin-coated onto FTO substrates at 1800 rpm for 30 s. Following this, the substrates underwent crucial annealing at 150  $^\circ\text{C}$  for 10 min, enhancing the perovskite quality in the PSC. The process concluded with the deposition of a thick layer of silver through sputtering at a rate of 0.3 nm/s. Commonly, traditional device setups employ a  $\text{TiO}_2$  layer, often requiring high-temperature calcination to enhance its properties. That approach, though effective, faces issues of thermal stability and defects. In this innovative method, skipping the  $\text{TiO}_2$  layer eliminates the high-temperature steps, simplifying fabrication and reducing the structural risks due to heat. By deviating from the traditional method of including a compact or mesoscopic  $\text{TiO}_2$  layer, this proposed approach provides a new avenue for designing more efficient PSCs.

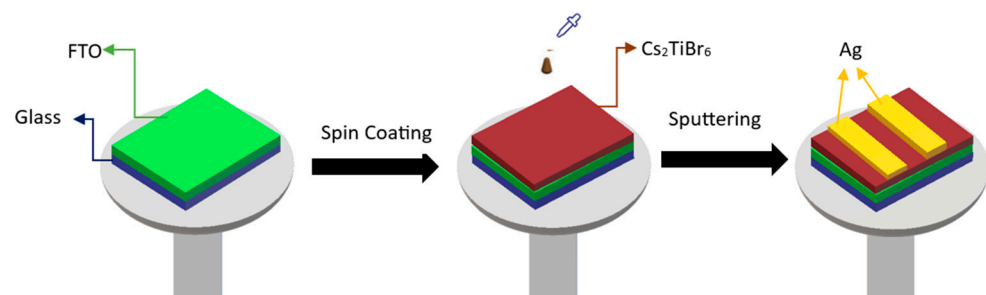


Figure 1. Steps for fabricating the proposed PSC.

## 2.2. Synthesis of Graphene Quantum Dots (GQDs) and Modified PSC Structure (FTO/GQDs/Cs<sub>2</sub>TiBr<sub>6</sub>/Ag)

The synthesis of the graphene quantum dots (GQDs) involved dispersing 270 mg of graphene oxide (GO) in 30 mL of N,N-Dimethylformamide (DMF). Following 30 min of ultrasonication, the solution underwent heating at 200 °C in a Teflon-lined autoclave for 8 h. Subsequently, it was cooled to room temperature, resulting in the formation of a brown, transparent suspension.

For the fabrication of the device, the GQDs were spin-coated onto fluorine-doped tin oxide (FTO) at 1400 rpm for 40 s, followed by a 75 °C, 25 min thermal treatment prior to perovskite deposition. This strategic enhancement led to the formation of a remarkable FTO/GQDs/Cs<sub>2</sub>TiBr<sub>6</sub>/Ag device, which exhibited notable improvements in its photovoltaic parameters, as discussed in the next section.

## 3. Results

A comprehensive characterization of the intrinsic properties of the Cs<sub>2</sub>TiBr<sub>6</sub> was performed, as depicted in Figure 2a–f. Figure 2a presents the TEM image of the Cs<sub>2</sub>TiBr<sub>6</sub>, showcasing a remarkably dense and uniform surface morphology. The XRD analysis of the Cs<sub>2</sub>TiBr<sub>6</sub> in Figure 2b shows clear 2θ peaks at 29.2°, 31°, 46°, and 56.2°, revealing its crystallographic properties. Figure 2c showcases the optical absorbance curves of the Cs<sub>2</sub>TiBr<sub>6</sub> absorber on the FTO [11]. These data confirm the absorber's efficacy in capturing sunlight with wavelengths of shorter than 430 nm. This suggests that the operational spectrum is primarily within the blue light range of the visible light spectrum and there is restricted light material interaction in the other light ranges. In Figure 2d, a plot of  $(\alpha h\nu)^2$  versus energy ( $h\nu$ ) is presented, allowing for the calculation of the bandgap of the Cs<sub>2</sub>TiBr<sub>6</sub>. The calculated bandgap value was confirmed to be 1.8 eV, falling within the suitable range for the absorber's electronic properties [10].

Figure 2e shows the band diagram of the proposed PSCs without ETL or HTL, depicting the energy level alignment and the electronic transitions governing the photovoltaic behavior. The subsequent investigation of the FTO/Cs<sub>2</sub>TiBr<sub>6</sub>/Ag device's cross-sectional structure, i.e., the SEM results, are illustrated in Figure 2f. This examination revealed a vertically oriented architecture, with the Cs<sub>2</sub>TiBr<sub>6</sub> layer aligned in a monolayer configuration. This layer possessed a thickness of 290 nm, and it was capped with a thick Ag layer.

The J-V curve was measured using a Keithley 2400 unit under simulated AM 1.5 G sunlight to replicate real solar conditions (light intensity of  $\cong 100 \text{ mW/cm}^2$ ). In Figure 3b, the comparative J-V curves of both the proposed PSCs are displayed. The FTO/Cs<sub>2</sub>TiBr<sub>6</sub>/Ag device achieved a J<sub>sc</sub> of  $1.78 \text{ mA cm}^{-2}$ , a V<sub>oc</sub> of 0.55 V, an FF of 44.2% and a PCE of 0.89%, which were calculated using Equations (1) and (2). The inefficiency of the present design arises from a significant energy barrier between the FTO's work function (−4.4 eV) and Cs<sub>2</sub>TiBr<sub>6</sub>'s CB (−4.0 eV), causing recombination and poor extraction [12,13]. To counter this, graphene quantum dots (GQDs) were introduced [14,15] and a modified PSC structure (FTO/GQDs/Cs<sub>2</sub>TiBr<sub>6</sub>/Ag) was developed, as was discussed in the previous section. The TEM image of the synthesized GQD is shown in Figure 3a.

$$F = P_{\max} / (V_{\text{oc}} \times J_{\text{sc}}) \quad (1)$$

$$\text{PCE} = \frac{(V_{\text{oc}} \times J_{\text{sc}} \times \text{FF})}{P_{\text{in}}} \quad (2)$$

To confirm an enhanced photocurrent, we assessed the incident photon-to-current conversion efficiency (IPCE) spectra, shown in Figure 3c. A marked IPCE enhancement appeared from 380 to 550 nm when a GQD layer was inserted between the perovskite and FTO layers. Through the integration of the GQDs into the PSC structure, the maximum IPCE rose from 34.6% to 38.79%, along with the J<sub>sc</sub> rising from  $1.78 \text{ mA cm}^{-2}$  to  $1.95 \text{ mA cm}^{-2}$ , whereas the fill factor (FF) and open-circuit voltage (V<sub>oc</sub>) values were almost similar. The

$\Delta$ IPCE data, which represented the internal quantum efficiency spectra, demonstrated a notable improvement, especially around 510 nm, attributed to the inclusion of the GQDs. This enhancement was predominantly driven by the absorption of the perovskite's excited state within the GQD layers, in line with the expected minimal absorption by the GQD monolayers [16]. As a result, the introduction of the GQDs streamlined the electron extraction, reduced trapping, and yielded an overall efficiency boost that remained consistent across the visible spectrum.

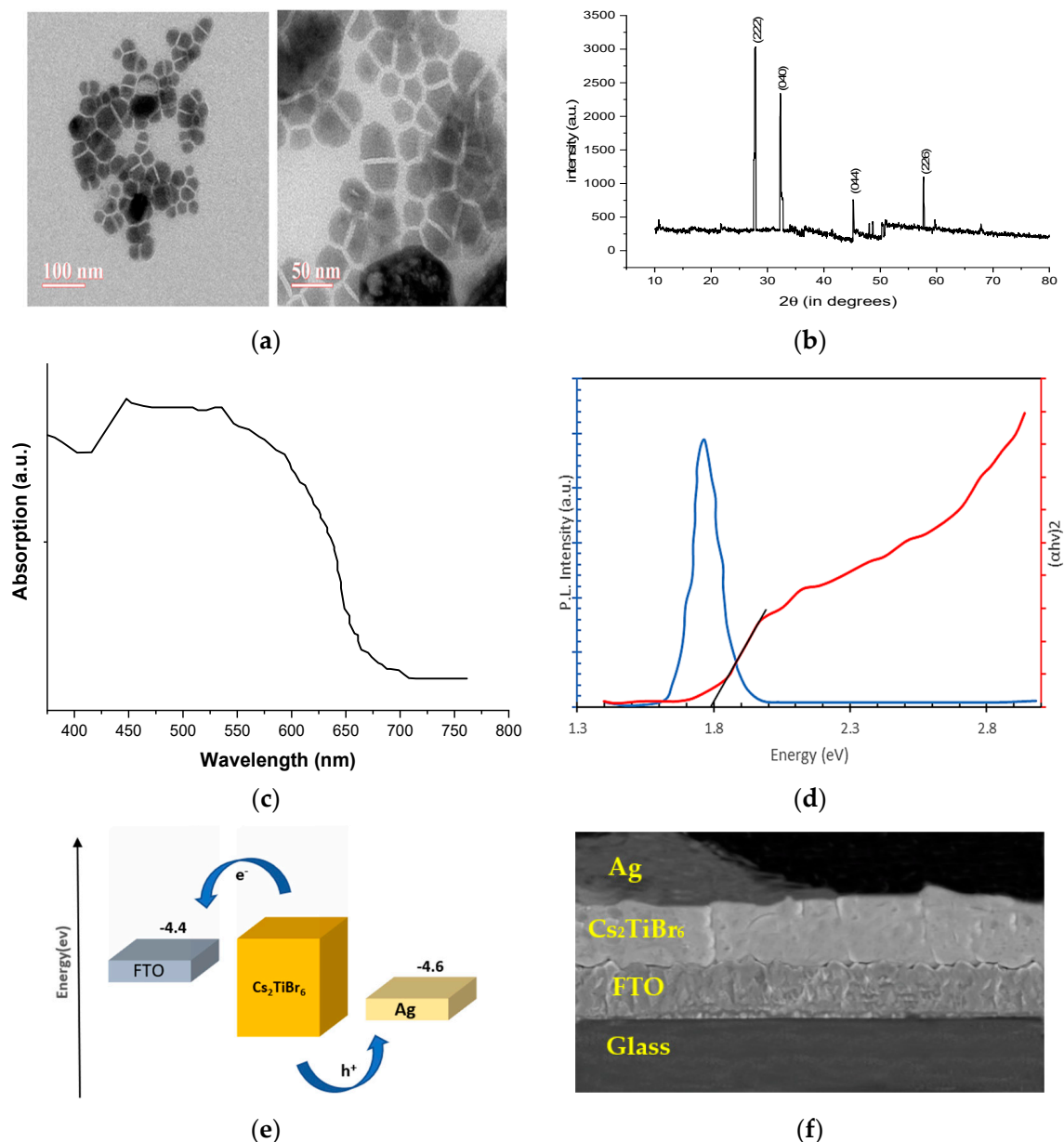


**Figure 2.** (a) TEM results for synthesized perovskite. (b) XRD results for synthesized perovskite. (c) UV–Vis results for synthesized perovskite. (d) PL spectrum and Tauc plot of PSC. (e) Energy band diagram of PSC. (f) SEM results of PSC.

To analyze the GQDs' charge extraction behavior, optical characterizations were performed on various  $\text{Cs}_2\text{TiBr}_6$  films. Emission light intensity correlates with radiative recombination between photogenerated electrons and induced holes. The steady-state photoluminescence (PL) spectrum evaluates charge extraction kinetics. In Figure 3d, the PL spectra of glass/ $\text{Cs}_2\text{TiBr}_6$ /Ag show a centered peak at 580 nm. The peak intensity deviates in the structure with the GQDs. PL peaks are lacked due to the weaker light conversion than in

$\text{Cs}_2\text{TiBr}_6$ . The significant decrease in photoluminescence resulted from an improved charge extraction facilitated by the GQDs. This addition enhanced charge transport, thereby mitigating the recombination of photoexcited carriers and lowering photoluminescence emission.

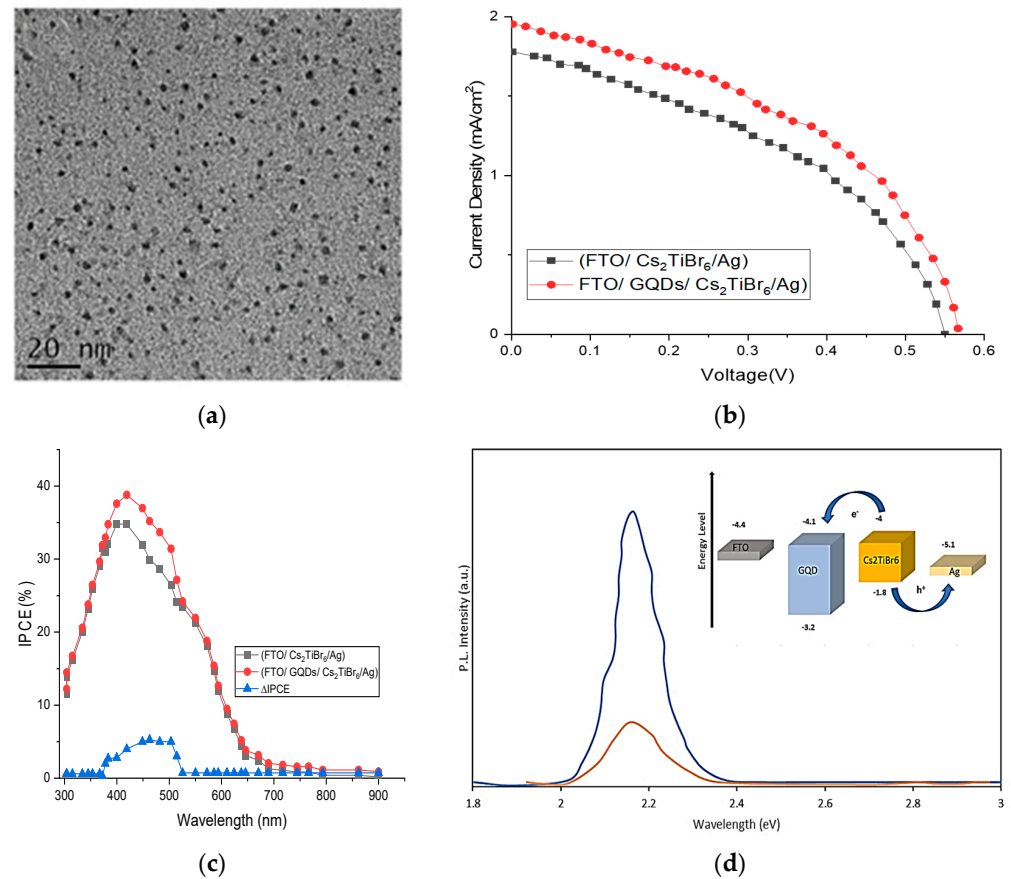


**Figure 3.** (a) TEM image of GQD. (b) J–V curve. (c) IPCE graph. (d) PL spectra of proposed structure.

The evaluated performances of the PSCs both with and without the incorporation of the graphene quantum dots (GQDs) are shown in Table 1. The structure incorporating GQDs displayed notable improvements: the  $J_{sc}$ ,  $V_{oc}$ , and FF increased to  $1.95 \text{ mA cm}^{-2}$ , 0.57 V, and 45.1%, respectively, leading to a PCE of 1.02%. These enhancements can be attributed to enhanced electron extraction, improved charge transport, favorable energy levels, and reduced charge carrier recombination at the interface.

**Table 1.** Outcomes of the proposed PSC configuration.

Shape	$V_{oc}$ (V)	FF (%)	$J_{sc}$ ( $\text{mA cm}^{-2}$ )	PCE (%)
FTO/ $\text{Cs}_2\text{TiBr}_6$ /Ag	0.55	44.2	1.78	0.89
FTO/GQDs/ $\text{Cs}_2\text{TiBr}_6$ /Ag	0.57	45.1	1.95	1.02

#### 4. Conclusions

In summary, our study introduces  $\text{Cs}_2\text{TiBr}_6$  as a promising lead-free perovskite material for solar cells. We utilized a simple spin-coating method to fabricate PSCs with and without GQDs. These PSCs exhibited notable characteristics, including a high open-circuit voltage ( $V_{oc}$ ) of 0.57 V and a commendable FF of 45.10. Although the efficiency was 1.02%, we believe it can be improved by optimizing the film thickness, refining the surface quality, and enhancing the electrical contacts in future iterations. Additionally, the use of  $\text{Cs}_2\text{TiBr}_6$  as an absorber layer without the need for ETL or HTL has positioned it as a promising

choice for future lead-free perovskite solar cell technology. This approach aligns with our commitment to sustainable and environmentally friendly solar energy solutions.

**Author Contributions:** R.S. was responsible for generating the concepts, fabrication, noting the results, and preparing the initial draft. M.Y. provided valuable suggestions during this work and made corrections in the draft. All authors have read and agreed to the published version of the manuscript.

**Funding:** This research received no external funding.

**Institutional Review Board Statement:** Not applicable.

**Informed Consent Statement:** Not applicable.

**Data Availability Statement:** Data are contained within the article.

**Conflicts of Interest:** The authors declare no conflicts of interest.

## References

1. Jung, H.S.; Park, N.G. Perovskite solar cells: From materials to devices. *Small* **2015**, *11*, 10–25. [\[CrossRef\]](#) [\[PubMed\]](#)
2. Song, T.-B.; Chen, Q.; Zhou, H.; Jiang, C.; Wang, H.-H.; Yang, Y.M.; Liu, Y.; You, J. Perovskite solar cells: Film formation and properties. *J. Mater. Chem. A* **2015**, *3*, 9032–9050. [\[CrossRef\]](#)
3. Grätzel, M. The light and shade of perovskite solar cells. *Nat. Mater.* **2014**, *13*, 838–842. [\[CrossRef\]](#) [\[PubMed\]](#)
4. Park, N.-G. Perovskite solar cells: An emerging photovoltaic technology. *Mater. Today* **2015**, *18*, 65–72. [\[CrossRef\]](#)
5. Kim, J.Y.; Lee, J.W.; Jung, H.S.; Shin, H.; Park, N.G. High-efficiency perovskite solar cells. *Chem. Rev.* **2020**, *120*, 7867–7918. [\[CrossRef\]](#) [\[PubMed\]](#)
6. Bati, A.S.R.; Zhong, Y.L.; Burn, P.L.; Nazeeruddin, M.K.; Shaw, P.E.; Batmunkh, M. Next-generation applications for integrated perovskite solar cells. *Commun. Mater.* **2023**, *4*, 2. [\[CrossRef\]](#)
7. Huang, Y.; Liu, T.; Liang, C.; Xia, J.; Li, D.; Zhang, H.; Amini, A.; Xing, G.; Cheng, C. Towards Simplifying the Device Structure of High-Performance Perovskite Solar Cells. *Adv. Funct. Mater.* **2020**, *30*, 2000863. [\[CrossRef\]](#)
8. Duan, J.L.; Zhao, Y.Y.; He, B.L.; Tang, Q.W. Simplified perovskite solar cell with 4.1% efficiency employing inorganic CsPbBr<sub>3</sub> as light absorber. *Small* **2018**, *14*, 1704443. [\[CrossRef\]](#) [\[PubMed\]](#)
9. Yin, X.; Zhai, J.; Song, L.; Du, P.; Li, N.; Yang, Y.; Xiong, J.; Ko, F.K. Novel NiO Nanoforest Architecture for Efficient Inverted Mesoporous Perovskite Solar Cells. *ACS Appl. Mater. Interfaces* **2019**, *11*, 44308–44314. [\[CrossRef\]](#) [\[PubMed\]](#)
10. Grandhi, G.K.; Matuhina, A.; Liu, M.; Annurakshita, S.; Ali-Löyty, H.; Bautista, G.; Vivo, P. Lead-Free Cesium Titanium Bromide Double Perovskite Nanocrystals. *Nanomaterials* **2021**, *11*, 1458. [\[CrossRef\]](#) [\[PubMed\]](#)
11. Chen, M.; Ju, M.-G.; Carl, A.D.; Zong, Y.; Grimm, R.L.; Gu, J.; Zeng, X.C.; Zhou, Y.; Padture, N.P. Cesium Titanium(IV) Bromide Thin Films Based Stable Lead-free Perovskite Solar Cells. *Joule* **2018**, *2*, 558–570. [\[CrossRef\]](#)
12. Baena, J.P.C.; Steier, L.; Tress, W.; Saliba, M.; Neutzner, S.; Matsui, T.; Giordano, F.; Jacobsson, T.J.; Kandada, A.R.S.; Zakeeruddin, S.M.; et al. Highly efficient planar perovskite solar cells through band alignment engineering. *Energy Environ. Sci.* **2015**, *8*, 2928–2934. [\[CrossRef\]](#)
13. Dong, J.; Shi, J.; Li, D.; Luo, Y.; Meng, Q. Controlling the conduction band offset for highly efficient ZnO nanorods based perovskite solar cell. *Appl. Phys. Lett.* **2015**, *107*, 073507. [\[CrossRef\]](#)
14. Gan, X.; Yang, S.; Zhang, J.; Wang, G.; He, P.; Sun, H.; Yuan, H.; Yu, L.; Ding, G.; Zhu, Y. Graphite-N Doped Graphene Quantum Dots as Semiconductor Additive in Perovskite Solar Cells. *ACS Appl. Mater. Interfaces* **2019**, *11*, 37796–37803. [\[CrossRef\]](#) [\[PubMed\]](#)
15. Acik, M.; Darling, S.B. Graphene in perovskite solar cells: Device design, characterization and implementation. *J. Mater. Chem. A* **2016**, *4*, 6185–6235. [\[CrossRef\]](#)
16. Zhu, Z.; Ma, J.; Wang, Z.; Mu, C.; Fan, Z.; Du, L.; Bai, Y.; Fan, L.; Yan, H.; Phillips, D.L.; et al. Efficiency Enhancement of Perovskite Solar Cells through Fast Electron Extraction: The Role of Graphene Quantum Dots. *J. Am. Chem. Soc.* **2014**, *136*, 3760–3763. [\[CrossRef\]](#) [\[PubMed\]](#)

**Disclaimer/Publisher's Note:** The statements, opinions and data contained in all publications are solely those of the individual author(s) and contributor(s) and not of MDPI and/or the editor(s). MDPI and/or the editor(s) disclaim responsibility for any injury to people or property resulting from any ideas, methods, instructions or products referred to in the content.